iScience

CellPress
OPEN ACCESS

Article

Antibody specificity against highly conserved membrane protein Claudin 6 driven by single atomic contact point

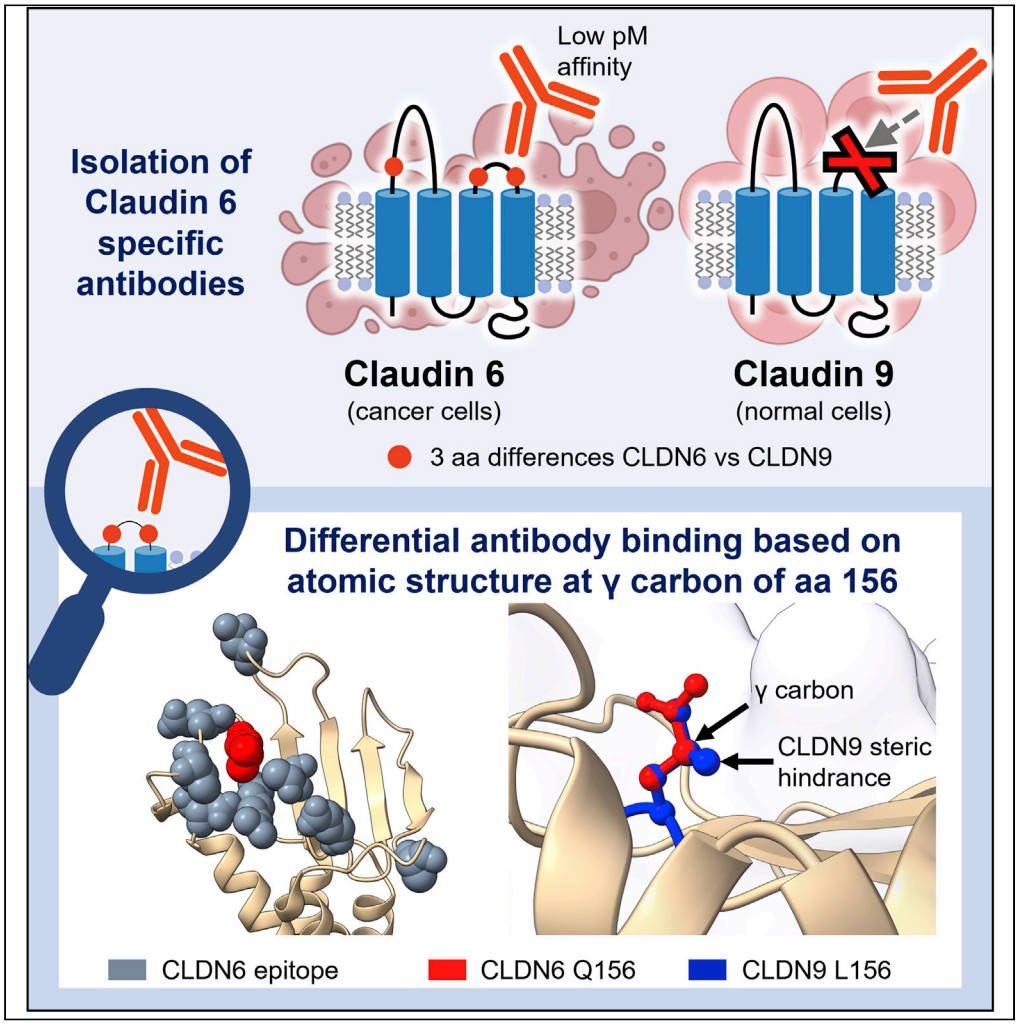

Brad Screnci, Lewis J. Stafford, Trevor Barnes, ..., Benjamin J. Doranz, Joseph B. Rucker, Ross Chambers

rchambers@integralmolecular.com

Highlights

High affinity antibodies isolated against the oncology target claudin 6

Antibodies show no cross-reactivity to claudin 9 or 22 other claudin family members

Atomic-level epitope mapping identifies the γ carbon on Q156 as enabling specificity

Humanized antibody candidates are selected with good developability

Screnci et al., iScience *25*, 105665
December 22, 2022
https://doi.org/10.1016/j.isci.2022.105665

iScience

CellPress
OPEN ACCESS

Article

Antibody specificity against highly conserved membrane protein Claudin 6 driven by single atomic contact point

Brad Screnci,[1] Lewis J. Stafford,[1] Trevor Barnes,[1] Kristen Shema,[1] Samantha Gilman,[1] Rebecca Wright,[1] Suzie Al Absi,[1] Tim Phillips,[1] Charles Azuelos,[1] Katherine Slovik,[1] Paige Murphy,[1] Daniel B. Harmon,[1] Tom Charpentier,[1] Benjamin J. Doranz,[1] Joseph B. Rucker,[1] and Ross Chambers[1,2,*]

SUMMARY

The tight junction protein claudin 6 (CLDN6) is differentially expressed on cancer cells with almost no expression in healthy tissue. However, achieving therapeutic MAb specificity for this 4 transmembrane protein is challenging because it is nearly identical to the widely expressed CLDN9, with only 3 extracellular amino acids different. Most other CLDN6 MAbs, including those in clinical development are cross-reactive with CLDN9, and several trials have now been stopped. Here we isolated rare MAbs that bind CLDN6 with up to picomolar affinity and display minimal cross-reactivity with CLDN9, 22 other CLDN family members, or across the human membrane proteome. Amino acid-level epitope mapping distinguished the binding sites of our MAbs from existing clinical-stage MAbs. Atomic-level epitope mapping identified the structural mechanism by which our MAbs differentiate CLDN6 and CLDN9 through steric hindrance at a single molecular contact point, the γ carbon on CLDN6 residue Q156.

INTRODUCTION

Claudins (CLDNs) are a family of integral transmembrane proteins that play a critical role in regulating the permeability of tight junctions, the cell-cell adhesion complexes that mediate polarity, proliferation, and differentiation of epithelial and endothelial cells.[1] Loss of tight junction integrity is critical for the diffusion of nutrients and other factors that support tumor growth and survival.[2] In addition, loss of cell-cell adhesion, polarity, and differentiation are important steps in the progression toward metastasis.[2,3] Dysregulated expression of CLDNs has been documented in the majority of solid tumor malignancies.[4]

CLDN6, one of the 24 known human CLDN family members, has garnered considerable attention as a potential oncotherapeutic target because of its high and specific expression in many solid tumors (Figure S1A). Most human CLDNs are widely expressed, but CLDN6 is nearly exclusively found in solid tumors, with minimal or no expression in healthy adult tissue.[5–15] CLDN6 is among the first proteins to be expressed in embryonic stem cells committed to an epithelial fate and coincides with expression of the early epithelial marker keratin 8.[8,16] Expression of CLDN6 is restricted to endoderm-derived tissues in early embryonic development and to pluripotent stem cells.[5–7] In the healthy adult organism, CLDN6 is undetectable, but high expression has been observed in solid tumors, including ovarian, lung, endometrial, and gastric cancers (Figure 1A), as well as testicular cancer and teratomas.[8–15] In fact, 60% of ovarian, 65% of endometrial, and 95% of testicular cancers are CLDN6-positive.[20] CLDN6 expression remains elevated even after metastasis to distal cancer sites, and high levels of CLDN6 have been shown to correlate with tumor cell invasiveness, motility, and proliferation rate.[21,22] This differential expression suggests that CLDN6 is a viable target for biotherapeutics using a wide variety of modalities, including bispecific T cell engagers, CAR-T-cells, and antibody drug conjugates (ADCs). Because of the cytotoxic mechanisms of these modalities, off-target interactions have lead to substantial safety risks. CLDN6 MAbs with high specificity would be able to direct a therapeutic agent toward the tumor while minimizing interaction with healthy tissues.

Despite their potential, no therapeutics targeting CLDN6 have been approved to date. CLDN6 MAbs are difficult to isolate, in part due to the structural complexity of the antigen. Proteins in the CLDN family share

[1]Integral Molecular, 3711 Market Street, Suite 900, Philadelphia, PA 19104, USA

[2]Lead contact

*Correspondence: rchambers@integralmolecular.com

https://doi.org/10.1016/j.isci.2022.105665

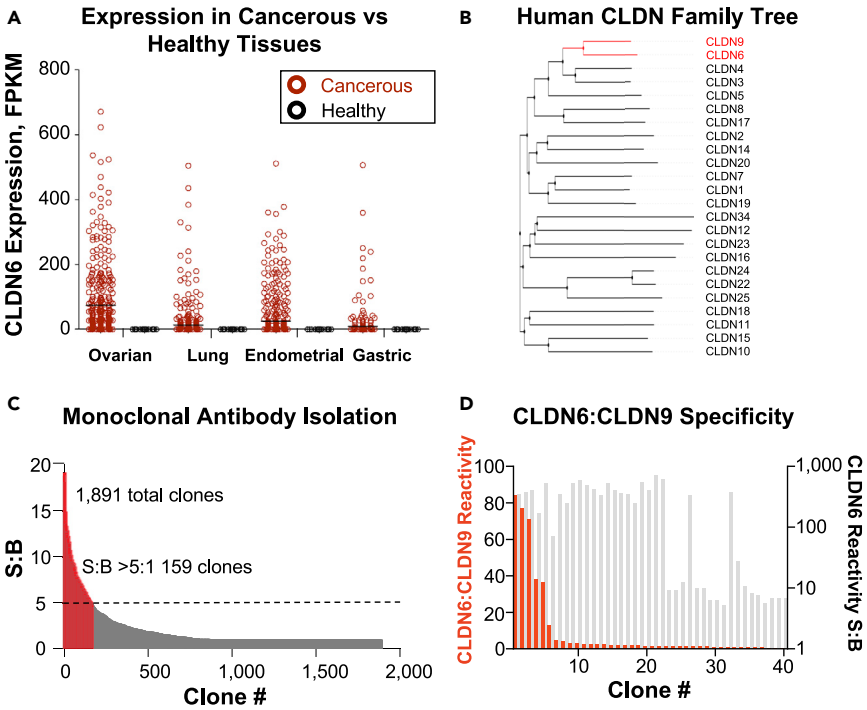

Figure 1. Isolation of highly specific CLDN6 MAbs

(A) CLDN6 is highly expressed in cancerous tissues and absent from healthy tissues. The Gene Expression Profiling Interactive Analysis (GEPIA) database[17] was queried for CLDN6 RNAseq expression data in cancerous and healthy tissue samples. Each datapoint represents one patient. Expression was measured in number of sequenced fragments per kilobase of transcript per million mapped reads (FPKM).

(B) Human protein sequences were retrieved from UniProt and aligned using ClustalOmega.[18] Simple Phylogeny was used to generate a tree based on the alignment, which was then displayed using iTol.[19]

(C) Isolated scFvs were tested for CLDN6 target specificity by flow cytometry. Individual clones displaying more than a 5:1 signal-to-background (S:B) ratio for CLDN6 are shown in red.

(D) Forty clones were screened in IgG format for CLDN6:CLDN9 selective binding by flow cytometry. Red bars show the ratio of CLDN6:CLDN9 binding signal for each individual antibody (left Y axis). Gray bars show S:B for CLDN6 binding of each individual antibody (right Y axis).

a four-transmembrane domain structure with two extracellular loops.[23] The first loop is ~50 residues long and contains charged residues implicated in the formation of charge-selective paracellular channels,[24] as well as two highly conserved cysteines that increase protein stability through an intramolecular disulfide bond.[25] The second loop is potentially involved in forming the strands that seal tight junctions through oligomerization of CLDNs from adjacent cells.[26] As with other multi-spanning membrane proteins, the need to access the CLDN6 antigen in its native conformation and at high concentrations limits conventional antibody discovery methods.

Human CLDNs share approximately 95% extracellular sequence homology with their mouse counterparts, necessitating the use of divergent species for immunization (Figure S1B). CLDN6 is also highly similar in structure and sequence to other members of the CLDN family that are widely expressed in healthy tissues (Figure 1B). In particular, the extracellular regions of CLDN6 and CLDN9 differ by only 3 amino acids. Expression of CLDN9 has been observed in normal adult skeletal muscle, bone, cardiovascular system, and brain, whereas the closely related CLDN3 and CLDN4 are also ubiquitously expressed at high levels.[7,27] To be viable as an oncotherapeutic, MAbs targeting CLDN6 must bind with high specificity, excluding CLDN9 and other closely related CLDNs. However, nearly all CLDN6 MAbs in clinical development to date have demonstrated significant cross-reactivity with the broadly expressed CLDN9, and most trials have now been stopped.

Here we isolated highly specific CLDN6 MAbs and identified their mechanism of specificity. We were able to isolate rare MAbs that selectively bind CLDN6 but show minimal cross-reactivity against CLDN9, other

CLDN family members, or any other membrane protein across the human genome. Flow cytometry on cells naturally expressing CLDN6 and with cell lines overexpressing CLDN proteins confirmed that these MAbs bound human, mouse, and cynomolgus CLDN6, with no binding to CLDN9. MAbs bound to CLDN6 with affinities as strong as 1 pM but displayed undetectable binding to CLDN9 when analyzed by biolayer interferometry. By individually mutating each of the 219 CLDN6 residues to alanine, we identified specific CLDN6 residues critical for MAb binding and differentiated these epitopes from existing MAbs in clinical development, which cross-react with other CLDN family members and have experienced safety issues in clinical trials. By comprehensively substituting residues of interest with all other possible residues, we identified steric hindrance of the γ carbon on Q156 as critical for absolute MAb specificity of CLDN6 versus CLDN9, defining the atomic-level mechanism of specificity for the MAbs we isolated here. This mechanism of specificity differs from other MAbs as it involves distinct residues involved in binding energetics versus steric hindrance.

RESULTS

Isolation of highly specific CLDN6 antibodies

To generate MAbs that strongly bind CLDN6, we used DNA and virus-like particles (Lipoparticles) incorporating CLDN6 in its native structure for immunization.[28] Membrane protein expression on the cell surface is often too low to induce a potent immune response needed to isolate a large panel of MAbs, but Lipoparticles allowed us to isolate structurally intact CLDN6 at protein concentrations 10- to 100-fold higher than typical commercial membrane preparations or intact cells.[28–31] Because CLDN6 is highly conserved in mouse, we used chickens as immunization hosts to take advantage of the evolutionary divergence between birds and mammals. Human CLDN6 has 88% overall sequence identity to mouse CLDN6 with 95% extracellular sequence identity and only 3 different extracellular residues, compared with 61% overall and 82% extracellular sequence identity and 14 different extracellular residues in its chicken paralog (CLDN4) (Figure S1B). This allowed us to bypass immune tolerance, which in a mammalian host typically results in a lower magnitude and diversity of immune response.

Using B cells from chickens with confirmed serum reactivity to CLDN6, we amplified antibody VH and VL gene fragments to construct a single-chain variable fragment (scFv) library.[32] To identify highly specific MAbs, the library was panned with CLDN6 Lipoparticles and deselected against CLDN9 Lipoparticles in three consecutive rounds, resulting in 1,891 unique reactive scFv fragments (Figure 1C). Each scFv was screened for CLDN6 binding by flow cytometry, identifying 159 fragments that bound with a signal-to-background (S:B) ratio of >5. The 40 strongest CLDN6 binders were selected to screen in IgG format for differential CLDN6 vs CLDN9 binding (Figure 1D). These screens identified 5 MAbs (IM136, IM170, IM171, IM172, and IM173) that bound CLDN6 with high specificity, as indicated by > 35-fold higher reactivity to CLDN6 compared with CLDN9. IM171 was humanized and affinity matured to generate MAbs IM301 and IM302, which became our lead candidates for further development. The 2 humanized MAbs, with IM136, IM171, IM172, and IM173 progressed to further characterization. For these 6 MAbs, the length of the heavy-chain complementarity-determining region 3 (VH CDR3)—the region primarily responsible for MAb specificity—ranged between 18 and 20 residues, which is longer than the majority of human- and mouse-derived MAbs and reflective of the longer VH CDR3 regions in chicken[33] (Table 1).

Isolated MAbs demonstrate high affinity and specificity for CLDN6

We selected six anti-CLDN6 MAbs and examined their reactivity and specificity in comparison to a panel of independently developed antibodies, all of which are at the clinical or preclinical stage. IMAB027 was in clinical development until recently for the treatment of advanced ovarian and testicular cancers (NCT02054351, NCT03760081;[34]). IMAB206 has the same heavy chain sequence as IMAB027 and is being developed as a CLDN6-CD3 bispecific antibody (WO2018054484A1). AE49-11 was patented for treating solid tumors (US9274119B2).

To test for reactivity with CLDN6, CLDN9, CLDN3, or CLDN4, each target protein was overexpressed in HEK-293F cells and surface MAb binding was evaluated by flow cytometry (Figures 2A and S2A). All our MAbs demonstrated CLDN6 binding with no or minimal CLDN9 cross-reactivity, whereas most benchmark MAbs bound CLDN6 and CLDN9 with comparable strength (50% of maximum binding signal [EC50s], Table 1). IM172 and IM173 associated with CLDN4 at comparable EC50s to CLDN6 by flow cytometry, but subsequent biosensor experiments with superior sensitivity showed weak to very weak binding of these MAbs to CLDN4 (K_D 17 to 756 nM). Immunofluorescent staining of HEK-293F cells transfected with

Table 1. Key CLDN6 MAb characteristics

MAb	VH CDR3 length (Kabat)	CLDN6 binding	CLDN9 binding	CLDN3 binding	CLDN4 binding	Mouse CLDN6 binding	Cyno CLDN6 binding	Conformational epitope	Epitope Topology	Critical Epitope residues
IM136	19	1.5 ± 0.5	IB	IB	IB	Yes	Yes	Yes	Extracellular	E48, D68, R158
IM171	18	2.1 ± 0.5	IB	IB	IB	Yes	Yes	Yes	Extracellular	T33, N38, E48, A153, E154, R158
IM172	20	3.3 ± 0.6	IB	IB	3.7 ± 1.2	Yes	Yes	Yes	Extracellular	N38, E48, D146, V152, E154, Q156, R158
IM173	18	5.8 ± 0.9	IB	IB	2.2 ± 1.0	Yes	Yes	Yes	Extracellular	E48, Q156, R158
IM301	18	2.8 ± 0.8	IB	IB	IB	Yes	Yes	Yes	Extracellular	E48, E154, R158
IM302	18	1.0 ± 0.1	IB	IB	IB	Yes	Yes	Yes	Extracellular	E154, R158
Benchmarks										
IMAB027 (Ganymed/ Astellas)	8	0.36 ± 0.01	8 ± 2	IB	IB	Yes	Yes	Yes	Extracellular	F35, G37, S39
IMAB206 (Ganymed/ Astellas)	8	0.4 ± 0.1	28 ± 5	IB	IB	Yes	Yes	ND	Extracellular	F35, G37, S39
AE49-11 (Chugai-Seiyaku)	14	1.2 ± 0.2	2.5 ± 0.5	IB	5.3 ± 0.5	Yes	Yes	ND	Extracellular	F35, G37, N38, I40, V41, Q44, V45, V55, L151, Q156, R158

CLDN protein binding: Flow cytometry EC50 ± error, nM. Error refers to the error on the fitted parameter. IB, insufficient binding to reach 50% of maximum. ND, experiment not done.

CLDN6 followed by widefield imaging showed strong signal localized to the cell membrane for all MAbs (Figure 3).

We tested MAb reactivity with mouse and cynomolgus CLDN6, because these model organisms are commonly used in preclinical studies. Our MAbs were generally better or comparable to the benchmarks (Figures 2B and S2B). We also confirmed that the MAbs bind endogenously expressing CLDN6 in the human ovarian cancer cell lines OVCAR3, OV90, and PA-1, which are often used in cellular and animal models of tumorigenesis (Figures 2C and S2C).

Because we used Lipoparticles containing conformationally intact CLDN6 for immunization, we examined whether the resulting MAbs bound conformational epitopes. CLDN6 was denatured and run on an SDS-PAGE gel, then probed with each MAb. Binding was detected using an HRP-tagged secondary antibody, and a commercially available MAb recognizing a CLDN6 linear epitope served as a positive control. None of the MAbs bound denatured CLND6, suggesting that all six recognize conformationally complex epitopes (Figure S3).

Preliminary biophysical and biochemical characterization of IM301 and IM302 indicated low propensity for aggregation (92.8–97.5% monomer), and melting temperatures (67.3–67.9°C) and production yields (~0.5 mg/mL) within acceptable ranges for other clinically successful antibody-based therapies[35–37] (Figure S4). The MAbs do not contain any amino acid motifs of concern for developability (NG: deamidation, M or C: oxidation, N-linked glycosylation sites, DP: hydrolysis, or aspartic acid (D) in the H3 sequences, which can have implications for isomerization). These assessments suggest good developability for both lead molecules IM301 and IM302.

To further quantify target binding and specificity, we measured binding kinetics to CLDN proteins using biolayer interferometry, with biotinylated Lipoparticles containing structurally-intact CLDNs attached to the biosensor tip. Titration assays with each MAb were used to calculate affinities (K_D), with all six of our

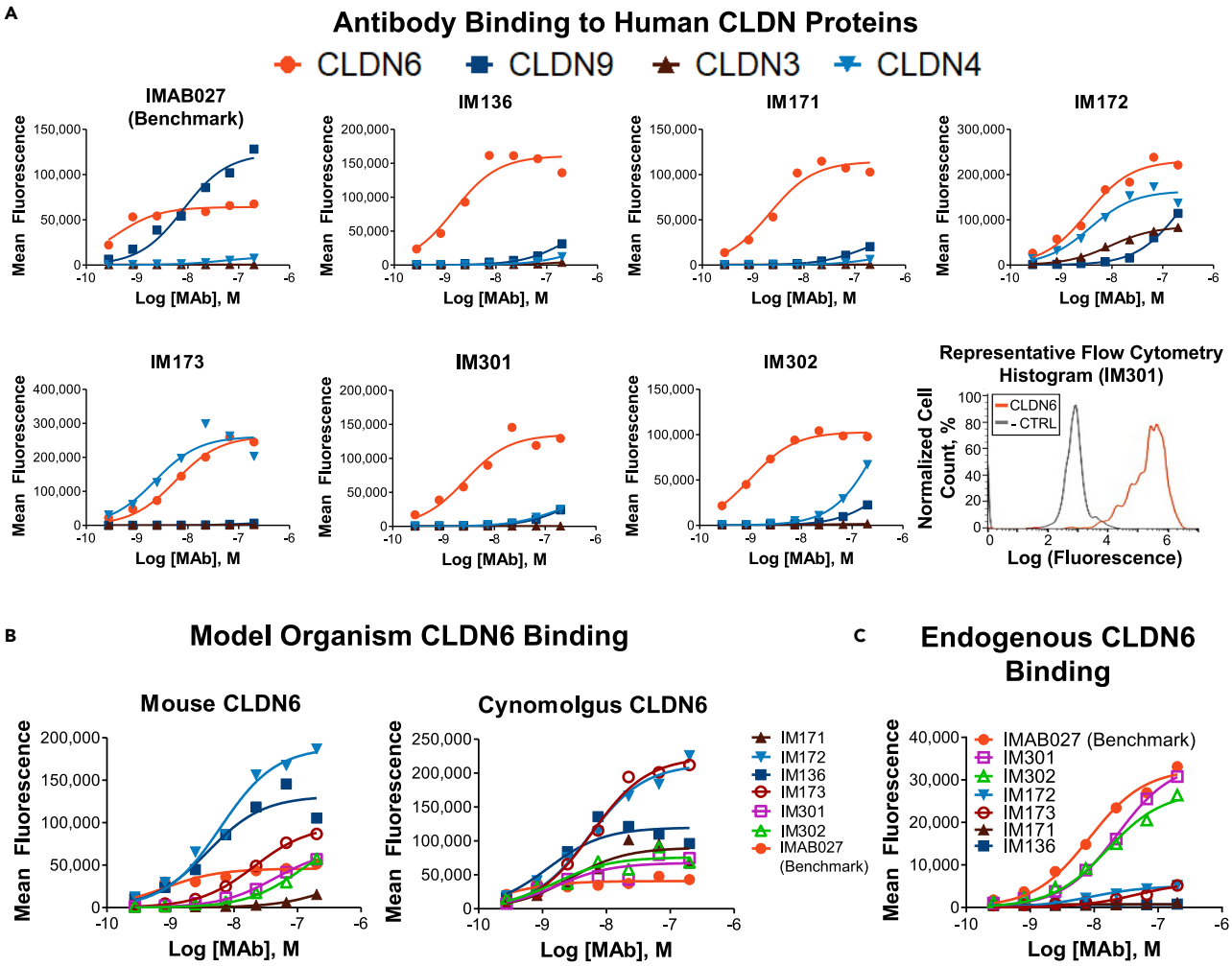

Figure 2. MAb reactivity and specificity for CLDN6

(A) HEK-293F cells were transfected with human CLDN6, CLDN9, CLDN3, or CLDN4 and stained with the indicated concentration of each MAb. A representative histogram from one data point (IM301) is shown.

(B) HEK-293F cells were transfected with mouse or cynomolgus CLDN6 orthologs.

(C) OVCAR3 human ovarian cancer cells were used to probe for MAb reactivity against endogenously expressed CLDN6. In all experiments, cells were stained with the indicated MAbs and surface binding was measured using flow cytometry. CLDN6 MAb IMAB027 (NCT02054351, Astellas) that was previously in clinical development served as a benchmark. Differences in maximum fluorescence represent target expression level and do not correlate directly with MAb affinity, as expression levels can vary for different CLDN family members.

MAbs demonstrating high affinity for CLDN6 (nanomolar range or better) (Figure 4 and Table 2). IM302 was an exceptionally strong CLDN6 binder, with K_D<1 pM. The benchmark MAbs IMAB027 and IMAB206 demonstrated strong CLDN9 cross-reactivity (affinities of 2–4 nM). The AE49-11 benchmark demonstrated detectable CLDN4 and CLDN9 off-target binding by biosensor assay, with affinities of 28–194 nM. Our MAbs demonstrated consistently very low CLDN9 cross-reactivity with affinities either undetectable or in the hundreds of nM. These biosensor analyses suggest that our MAbs possess a rare combination of strong CLDN6 affinity and exquisite specificity.

MAb specificity was further confirmed by screening each MAb against the human membrane proteome. The Membrane Proteome Array (MPA) consists of approximately 6,000 membrane proteins (94% of the human membrane proteome) expressed in their native state in unfixed cells.[38–41] Each MAb was added to the MPA and binding across the protein library was determined by flow cytometry, with positive hits being defined as more than three standard deviations (SD) above mean reactivity levels. The MPA screen further confirmed the CLDN6 reactivity of our MAbs. Because the MPA is screened with high MAb concentrations

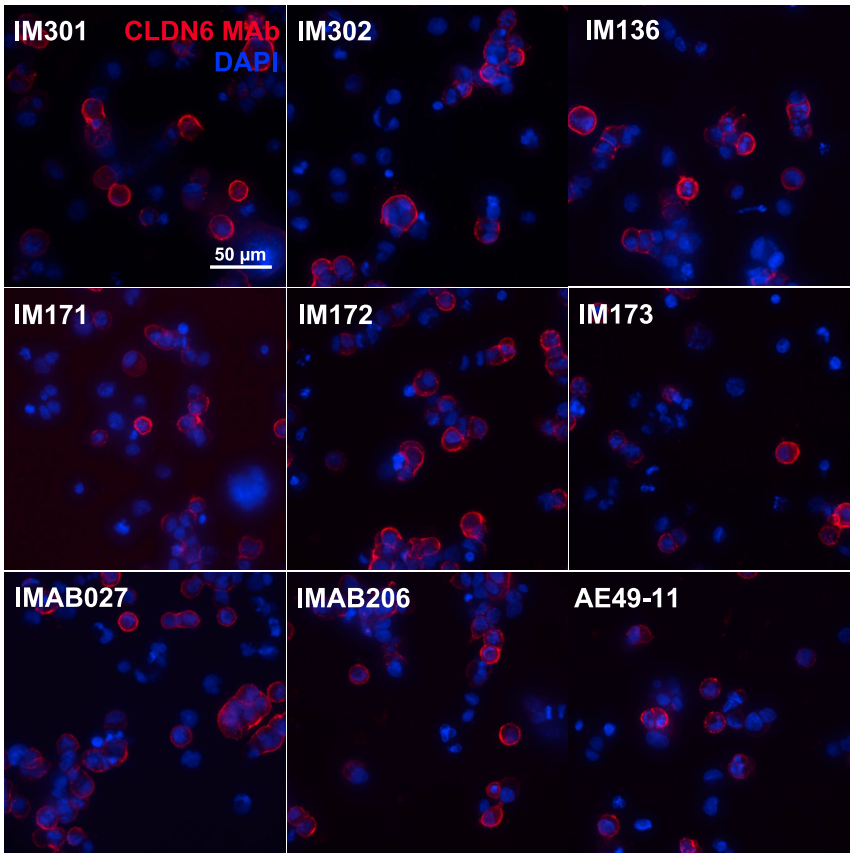

Figure 3. CLDN6 MAbs are cell membrane localized

HEK-293F cells were transfected with CLDN6, stained with the MAbs shown, as well as with DAPI nuclear stain, and visualized by immunofluorescence microscopy. Scale bar corresponds to 50 µm. IMAB027, IMAB206, and AE49-11 served as benchmark MAbs.

(5 µg/mL) to detect any possible off-target binding, low affinity cross-reactivity of some MAbs with CLDN4 and CLDN9 was also detected (Figures 5A and S5). These results suggest that the MPA can detect off-target reactivities even with very poor affinities (e.g., the K_D of IM172 binding to CLDN4 is 756 nM by biosensor but is still detectable on the MPA). The MPA is screened using permeabilized cells to further enhance sensitivity and also to detect all possible interactions, even for membrane proteins that may not traffic to the cell surface. Under permeabilized conditions, reactivity with the unrelated protein ABCC3 was detected for some MAbs. Follow-up experiments demonstrated that binding to ABCC3 was weak and entirely intracellular. MAbs bound to ABCC3 only when permeabilized, both in transfected HEK-293F cells and in endogenous A549 cells, with no detectable extracellular binding (Figures 5B and S6). The binding to an off-target, while not predictable (ABCC3 shares <4% identity with CLDN6, and the parental MAb IM171 did not bind ABCC3 before engineering), is not unusual, as our experience reveals that about 25% of MAbs demonstrate some off-target reactivity that can often be de-risked with extended validation.[42]

Together, the results from all binding assessments demonstrate the specificity of our MAbs compared with preclinical and clinical benchmarks, suggesting the potential of these MAbs to produce safer cancer therapeutics by avoiding off-target binding *in vivo*.

Epitope mapping reveals the amino acids critical for antibody binding

To better understand the mechanism by which these MAbs bind specifically to CLDN6, we identified the amino acid residues critical for the binding of each MAb. Using shotgun mutagenesis epitope mapping,[43] we performed a comprehensive alanine scan along the entire length of the 219 amino acid CLDN6 protein

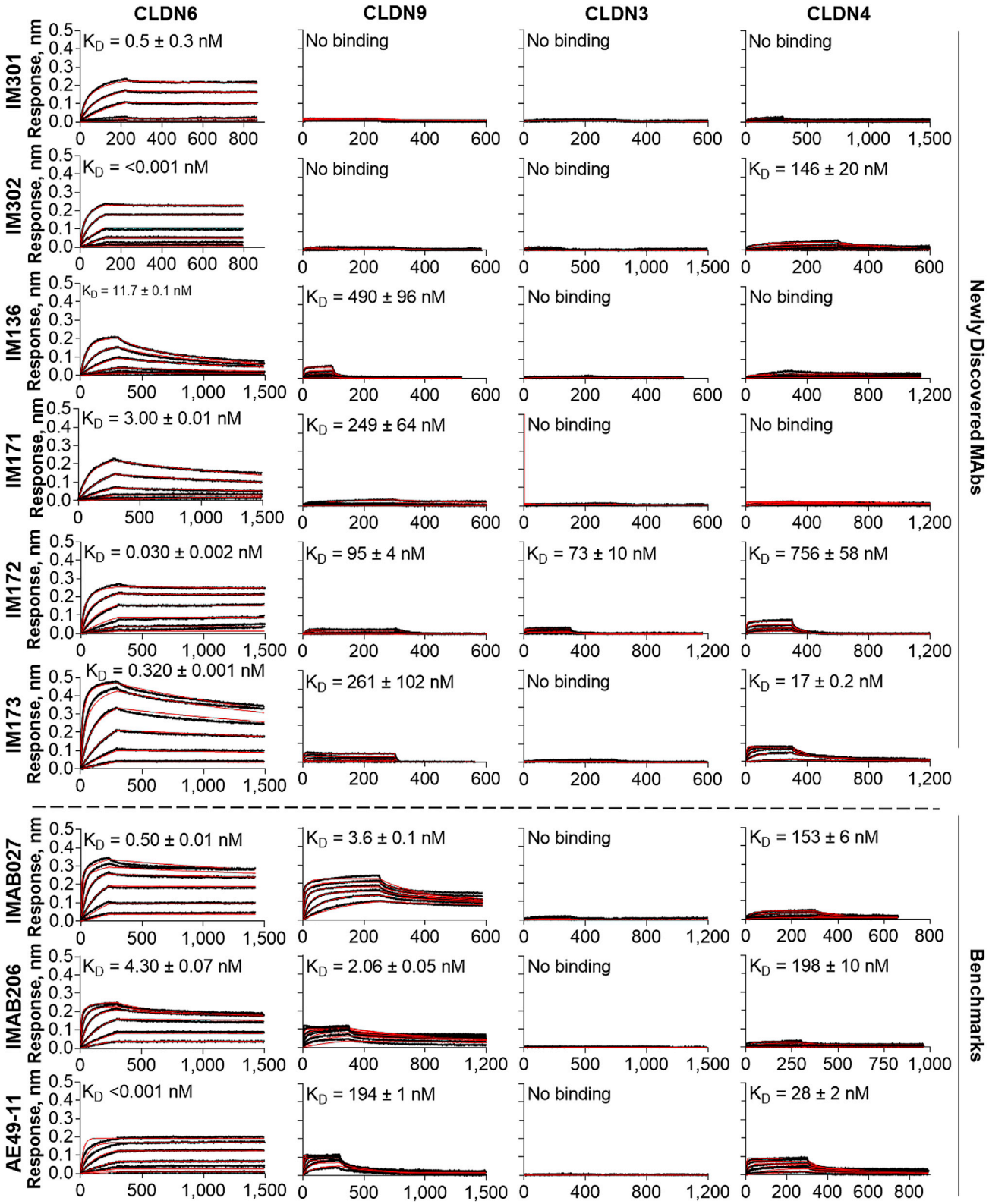
CLDN6
CLDN9
CLDN3
CLDN4
IM301
IM302
IM136
IM171
IM172
IM173
IMAB027
IMAB206
AE49-11
Response, nm
K_D = 0.5 ± 0.3 nM
No binding
No binding
No binding
K_D = <0.001 nM
No binding
No binding
K_D = 146 ± 20 nM
K_D = 11.7 ± 0.1 nM
K_D = 490 ± 96 nM
No binding
No binding
K_D = 3.00 ± 0.01 nM
K_D = 249 ± 64 nM
No binding
No binding
K_D = 0.030 ± 0.002 nM
K_D = 95 ± 4 nM
K_D = 73 ± 10 nM
K_D = 756 ± 58 nM
K_D = 0.320 ± 0.001 nM
K_D = 261 ± 102 nM
No binding
K_D = 17 ± 0.2 nM
K_D = 0.50 ± 0.01 nM
K_D = 3.6 ± 0.1 nM
No binding
K_D = 153 ± 6 nM
K_D = 4.30 ± 0.07 nM
K_D = 2.06 ± 0.05 nM
No binding
K_D = 198 ± 10 nM
K_D <0.001 nM
K_D = 194 ± 1 nM
No binding
K_D = 28 ± 2 nM
Newly Discovered MAbs
Benchmarks

Figure 4. Binding affinity for CLDN6 and structurally similar, widely expressed CLDNs

Biotinylated Lipoparticles incorporating native CLDN6, CLDN9, CLDN3, or CLDN4 were immobilized on biosensor tips (Forte Bio) and binding was measured for each MAb at the following concentrations: 66.7, 22.2, 7.40, 2.47, 0.800, and 0.267 nM for IM301, IM302, and benchmark MAbs on CLDN6; 33.3, 11.1, 3.70, 1.24, 0.412, and 0.137 nM for all other MAbs on CLDN6; 333, 111, 37.1, 12.3, 4.13, and 1.40 nM for all MAbs on CLDN9, CLDN3, or CLDN4. MAb binding kinetics were assessed by fitting data to a 1:2 binding model to determine the rate constants. Black curves represent the raw data and red curves represent the fitted traces.

(wild-type alanines were mutated to serines). We overexpressed each mutation in HEK-293T cells and tested each protein for MAb binding using high-throughput flow cytometry. Residues were considered critical for MAb binding if their mutation led to <35% binding signal relative to wild-type CLDN6. Mutants were also tested with a control commercial MAb (R&D Systems) to identify any mutations that affect local folding or protein expression.

This screening enabled us to identify specific residues critical for MAb binding to CLDN6 (Figure 6). Residue R158 was critical for the binding of all six MAbs, E154 was common for both humanized MAbs IM301 and IM302, and E48 was shared by all MAbs except IM302. Overall, the location of all critical epitope residues outlined a binding region near the apex of the two CLDN6 extracellular loops. These MAbs also displayed very different epitopes compared to those of the clinical benchmarks, which are not specific to CLDN6.

Atomic-level epitope mapping explains specificity for CLDN6

To further investigate the mechanism by which our MAbs differentiate CLDN6 from CLDN9, we used shotgun mutagenesis to map the CLDN6 epitope on an atomic level. The CLDN6 extracellular residues that differ from CLDN9 are M28 (L in CLDN9), R145 (Q), and Q156 (L). We mutated R145 and Q156 on CLDN6 to every other possible residue except cysteine, and tested for binding against IM171, IM301, and IM302. M28 was not included in this mapping, because it is located close to the transmembrane domain and away from the epitope sites uncovered by alanine scanning, suggesting it was unlikely to play a major role in MAb binding or specificity. Strikingly, most Q156 mutations almost completely abolished binding, suggesting that Q156 is the critical residue through which these MAbs differentiate between CLDN6 and CLDN9 (Figure 7A). Notably, Q156 lies in the center of the epitope footprint, surrounded by the critical residues identified by epitope mapping, but is not a direct contact residue (Figure 7B). In contrast, none of the R145 mutations led to substantial disruption of CLDN6 binding.

Mutating Q156 to alanine or glycine did not affect binding, suggesting that the residue at position 156 is important for MAb specificity because of steric rather than energetic factors. MAb binding was abolished by mutating Q156 to residues with branches from the β carbon (T, V, I, P) and γ carbon (L, D, N), suggesting that additional bulk in these locations sterically hinders MAbs from binding (Figure 7C). Because residue 156 is leucine in CLDN9, the γ carbon on Q156 appears to determine MAb specificity for CLDN6 versus CLDN9 (Figure 7D). Residues with longer or bulkier side chains than glutamine (K, R, F, Y, W, H) also disrupted binding, further indicating that steric hindrance at residue 156 defines the specificity for CLDN6 over CLDN9.

DISCUSSION

The high expression of CLDN6 in many solid tumor cancers, together with its complete absence from healthy adult tissues, makes CLDN6 a valuable oncotherapeutic target.[5–15] Yet the development of therapeutics targeting CLDN6 has been hindered by the difficulty of isolating highly specific CLDN6 MAbs. The protein's transmembrane structure and high conservation in mammals make immunization challenging. Exceptional MAb specificity is required to avoid cross-reactivity because of the high sequence and structural similarity of CLDN6 to widely expressed CLDN proteins, especially to CLDN9 whose extracellular sequence differs from CLDN6 at only 3 residues. We were able to bypass these challenges and isolate highly specific CLDN6 MAbs using strategies specifically tailored for antibody discovery against conserved and complex membrane proteins. Our MAbs were further shown to cross-react with mouse and cynomolgus CLDN6 that can facilitate downstream *in vivo* evaluation of efficacy and toxicity, which is usually difficult to achieve using mammalian immunization hosts because of immune tolerance.

Flow cytometry and biosensor experiments confirmed that the MAbs we isolated display minimal cross-reactivity with CLDN9, CLDN3, CLDN4, or any other human membrane protein. Biosensor measurements showed high affinity for native CLDN6, with IM302 demonstrating the highest affinity with K_D<1 pM, primarily driven by a very slow dissociation rate.

Table 2. MAb target binding kinetics measured using biolayer interferometry

	CLDN6			CLDN9			CLDN3			CLDN4		
MAb	K_D, nM	k_{on}, $nM^{-1}s^{-1}$	k_{off}, s^{-1}	K_D, nM	k_{on}, $nM^{-1}s^{-1}$	k_{off}, s^{-1}	K_D, nM	k_{on}, $nM^{-1}s^{-1}$	k_{off}, s^{-1}	K_D, nM	k_{on}, $nM^{-1}s^{-1}$	k_{off}, s^{-1}
IM136	11.7 ± 0.2	$2.3 \times 10^{-4} \pm 1.4\times10^{-6}$	$1.1 \times 10^{-3} \pm 2.8\times10^{-6}$	490 ± 96	$3.2 \times 10^{-4} \pm 1.8\times10^{-5}$	$1.5 \times 10^{-1} \pm 2.9\times10^{-2}$	No binding	No binding	No binding	No binding	No binding	No binding
IM171	3.00 ± 0.03	$1.6 \times 10^{-4} \pm 5.3\times10^{-7}$	$4.9 \times 10^{-4} \pm 3.7\times10^{-6}$	249 ± 64	$1.1 \times 10^{-5} \pm 1.9\times10^{-6}$	$2.7 \times 10^{-3} \pm 5.0\times10^{-4}$	No binding	No binding	No binding	No binding	No binding	No binding
IM172	0.030 ± 0.002	$6.8 \times 10^{-4} \pm 2.3\times10^{-6}$	$2.1 \times 10^{-5} \pm 1.6\times10^{-6}$	95 ± 4	1.6 × 10-4 ± 5.3×10-6	$1.5 \times 10^{-2} \pm 4.0\times10^{-4}$	73 ± 10	$3.3 \times 10^{-3} \pm 2.8\times10^{-4}$	$2.4 \times 10^{-1} \pm 2.7\times10^{-2}$	756 ± 58	$1.8 \times 10^{-4} \pm 5.4\times10^{-6}$	$1.3 \times 10^{-1} \pm 9.4\times10^{-3}$
IM173	0.320 ± 0.002	$1.1 \times 10^{-3} \pm 2.8\times10^{-6}$	$3.5 \times 10^{-4} \pm 2.0\times10^{-6}$	261 ± 102	$1.2 \times 10^{-3} \pm 3.0\times10^{-4}$	$3.0 \times 10^{-1} \pm 8.7\times10^{-2}$	No binding	No binding	No binding	17 ± 0.2	$3.7 \times 10^{-4} \pm 2.9\times10^{-6}$	$6.3 \times 10^{-3} \pm 5.1\times10^{-5}$
IM301	0.5 ± 0.03	$2.1 \times 10^{-4} \pm 2.8\times10^{-6}$	$1.2 \times 10^{-4} \pm 5.3\times10^{-6}$	No binding	No binding	No binding	No binding	No binding	No binding	No binding	No binding	No binding
IM302	<0.001	$4.0 \times 10^{-4} \pm 2.0\times10^{-6}$	$<1 \times 10^{-7}$	No binding	No binding	No binding	No binding	No binding	No binding	146 ± 20	$4.4 \times 10^{-5} \pm 3.3\times10^{-6}$	$6.3 \times 10^{-3} \pm 7.4\times10^{-4}$
Benchmarks												
IMAB027	0.50 ± 0.01	$6.9 \times 10^{-4} \pm 2.8\times10^{-6}$	3.4×10^{-4} 5.3×10^{-6}	3.6 ± 0.09	$1.2 \times 10^{-3} \pm 1.7\times10^{-5}$	$4.4 \times 10^{-3} \pm 8.4\times10^{-5}$	No binding	No binding	No binding	153 ± 6	$5.1 \times 10^{-5} \pm 1.3\times10^{-6}$	$7.8 \times 10^{-3} \pm 2.2\times10^{-4}$
IMAB206	4.30 ± 0.07	$5.2 \times 10^{-4} \pm 1.9\times10^{-6}$	$2.3 \times 10^{-3} \pm 3.7\times10^{-5}$	2.1 ± 0.05	$6.3 \times 10^{-4} \pm 9.9\times10^{-6}$	$1.3 \times 10^{-3} \pm 2.4\times10^{-5}$	No binding	No binding	No binding	198 ± 10	$3.6 \times 10^{-5} \pm 6.5\times10^{-7}$	$7.1 \times 10^{-3} \pm 3.4\times10^{-4}$
AE49-11	<0.001	Not measured	Not measured	194 ± 1	$7.4 \times 10^{-4} \pm 3.4\times10^{-6}$	$1.4 \times 10^{-1} \pm 7.5\times10^{-4}$	No binding	No binding	No binding	28 ± 2	$4.6 \times 10^{-4} \pm 1.0\times10^{-5}$	$1.3 \times 10^{-2} \pm 6.5\times10^{-4}$

Biosensor data were fit to a 1:2 binding model to determine the rate constants. Error shown is the error on the fitted parameter.

Having confirmed CLDN6 affinity and specificity, we investigated the mechanism through which the MAbs selectively bind CLDN6. We started by mapping epitopes at single amino acid resolution using shotgun mutagenesis comprehensive alanine scanning, which has been used to epitope map over 1,000 MAbs to date.[43] Our antibodies bind CLDN6 at a *trans*-interaction site in a tight junction so could in theory be blocked from MAbs access by tight junction formation. However, in tumors CLDN6 is highly up-regulated and although some of the molecules may be directly involved in tight junctions, many molecules will also be non-junctional and thus targeted by our antibodies. Because of the small size of the CLDN6 extracellular loops, lower-resolution epitope mapping methods would have binned all MAb epitopes to the same region or identified the overall footprint of the MAbs, but shotgun mutagenesis enabled us to identify the distinct residues critical for binding of each MAb.

Next, we characterized the atomic-level mechanism through which our MAbs differentiate between CLDN6 and CLDN9. We comprehensively mutated two of the three extracellular residues that differ between CLDN6 and CLDN9, because these residues were most likely to play a role in the specificity of our MAbs. We discovered that the γ carbon of residue 156 is critical for MAb differentiation between CLDN6 and CLDN9, with CLDN6-specific MAbs unable to bind proteins whose residue at position 156 contains branches from the γ carbon, including L156 in CLDN9. Mutating Q156 to residues with branches from the β carbon or with larger side chains than glutamine also prevented MAb binding to CDLN6, further suggesting that steric hindrance at residue 156 defines the specificity for CLDN6. Notably, specificity of these MAbs is achieved through a unique mechanism whereas target binding is carried out through energetically critical epitope residues that are conserved between CLDN6 and CLDN9, target specificity is accomplished through steric hindrance by residue 156, which is not directly involved in binding at all.

Unlike the MAbs discovered here, high MAb specificity is typically because of interactions that are also critical for target binding. For example, one study examined the crystal structure of the migraine drug erenumab in complex with the extracellular domains of its target CGRP receptor, comprising CLR and RAMP1.[44] RAMP1 is closely related to two other proteins, RAMP2 and RAMP3, each of which in complex with CLR confers specificity for a different target.[44] Erenumab was determined to be ~5,000 times more specific for CLR-RAMP1 than RAMP2/3, and this specificity was primarily because of interaction with residues on RAMP1 that were *not* conserved in RAMP2/3.[44] In another example, the anti-inflammatory drug canakinumab was demonstrated to recognize human IL-1β but not its rhesus or cynomolgus orthologs despite overall 96% sequence identity.[45] Structural studies uncovered the mechanistic difference as residue E64 on human IL-1β, which directly contacts residues in the canakinumab CDRs but is changed to a non-interacting alanine in rhesus and cynomolgus.[45] A similar mechanism of specificity conferred by binding-critical interactions has also been reported for MAbs with non-protein targets.[46,47] What is remarkable about the mechanism of MAb specificity uncovered in our current study of CLDN6 is that specificity is not determined by target binding (the same binding residues are present in both CLDN6 and CLDN9) but rather relies on steric block by the off-target.

Nearly all CLDN6 MAbs in clinical development to date have demonstrated significant cross-reactivity with the broadly expressed CLDN9, and most trials have now been stopped. The CLDN6 MAb IMAB027 (Astellas), which was used as a benchmark in our studies and displays significant cross-reactivity with CLDN9, underwent phase 1 trials for advanced ovarian cancer but is now halted from further clinical development.[34] Notably, an mRNA encoding a CLDN6/CD3 bi-(scFv)2 (BNT142) derived from the same sequence is still in active preclinical development (BioNTech).[48,49] A CAR-T cell therapy and an ADC (SC-004) were developed using a MAb with identical binding to CLDN6 and CLDN9, and demonstrated substantial safety issues in early clinical trials (AbbVie; US20170334991A1,[50]). Another CLDN6 MAb (Chugai; WO2021006328) has also been halted in clinical development, but its specificity has not been reported. In contrast to those benchmarks, CLDN6 MAb-based therapy BNT211 has demonstrated high specificity for CLDN6 so is in active clinical trials as an RNA vaccine for engineered CLDN6 CAR-T cells (BioNTech;[51]). Overall, previous efforts to develop CLDN6 MAbs suggest the need for specificity testing during the early stages of MAb discovery to avoid downstream safety issues severe enough to halt clinical development.

Using antibody isolation strategies tailored specifically for conserved and complex membrane proteins, we were able to isolate rare MAbs that bind the oncofetal target CLDN6 without off-target binding to the closely related and widely expressed CLDN9. Because of their specificity, the MAbs isolated and characterized in this study can be further incorporated into various cell-killing therapeutic modalities to target CLDN6, including antibody-drug conjugates (ADCs) and T cell redirection-based therapies such as

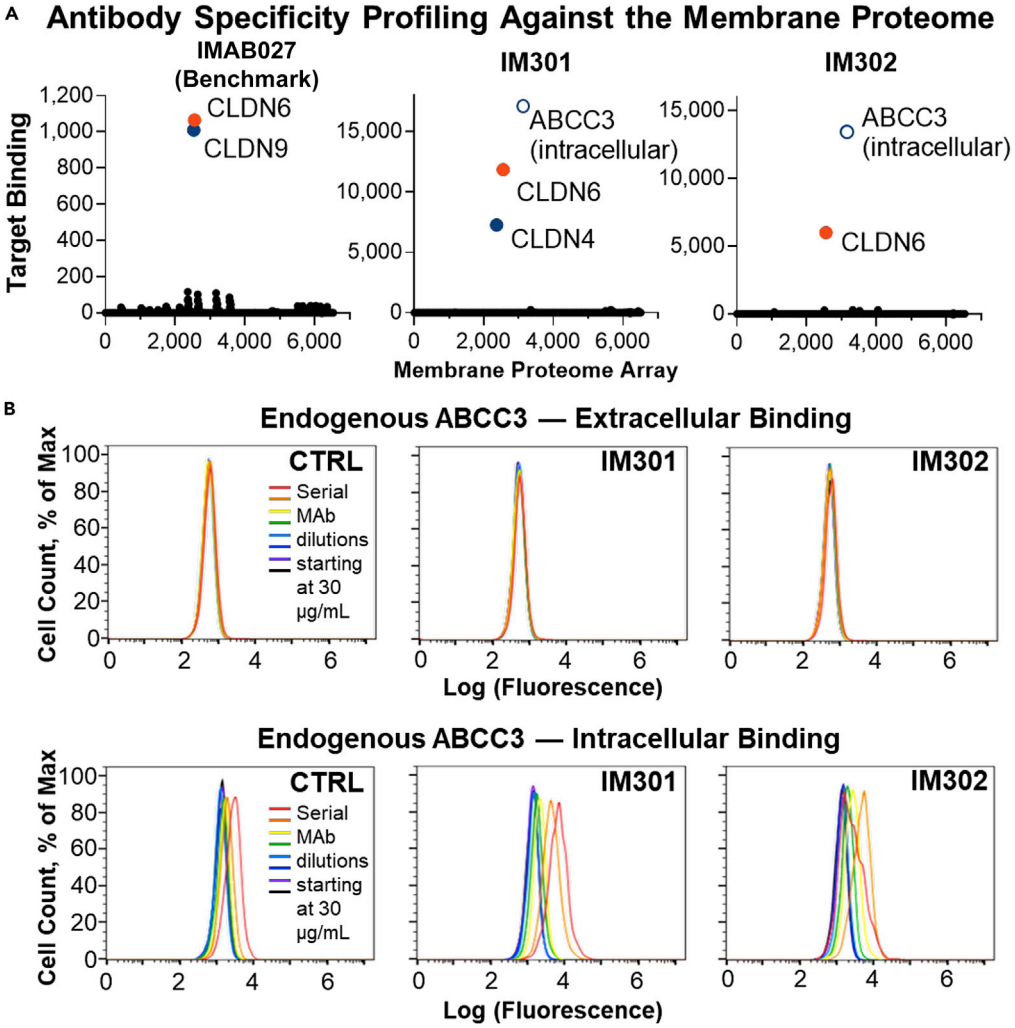

Figure 5. Membrane proteome-wide testing shows specificity of CLDN6 MAbs

(A) MAbs were screened for specificity using Integral Molecular's Membrane Proteome Array, consisting of ~6,000 human membrane proteins in their native state in unfixed cells. Antibody binding was detected by flow cytometry, and hits were defined as a binding signal more than 3 standard deviations higher than background and validated in follow-up assays. Unlabeled black dots represent hits that were below the defined threshold or that did not validate on retesting.

(B) MAb binding to ABCC3 is intracellular. IM301, IM302, and a control antibody (anti-P2X3) were tested for binding to ABCC3 endogenously expressed in A549 cells using 8 serial 3-fold antibody dilutions starting at 30 µg/mL (red). To detect intracellular binding, cells were permeabilized before testing for reactivity. Binding was measured using flow cytometry with a fluorescently labeled secondary antibody diluted 1:500.

CAR-T cell therapies or bispecific T cell engaging antibodies. These modalities have demonstrated potency in cancer clinical studies but are associated with substantial safety concerns because of the ramifications of off-target binding.[52–55] Atomic-level epitope mapping determined the mechanism of specificity exhibited by our MAbs to be a single side-chain contact whose steric hindrance, but not binding energetics, determines the ability to bind CLDN6 but not CLDN9. The high affinity and specificity of these MAbs for CLDN6, particularly IM301 and IM302, suggest their potential as safe and effective solid tumor therapeutics.

LIMITATIONS OF THE STUDY

The clinical benchmarks used in our studies, IMAB206, IMAB207, and AE49-11, are not derived from the original manufacturer and were produced for this research study based on the published sequence of their antibody variable chains. Thus, the clones used in our study are biosimilars and are not identical to the MAbs formulated for clinical development, especially in the Fc region (produced here with human IgG1), although

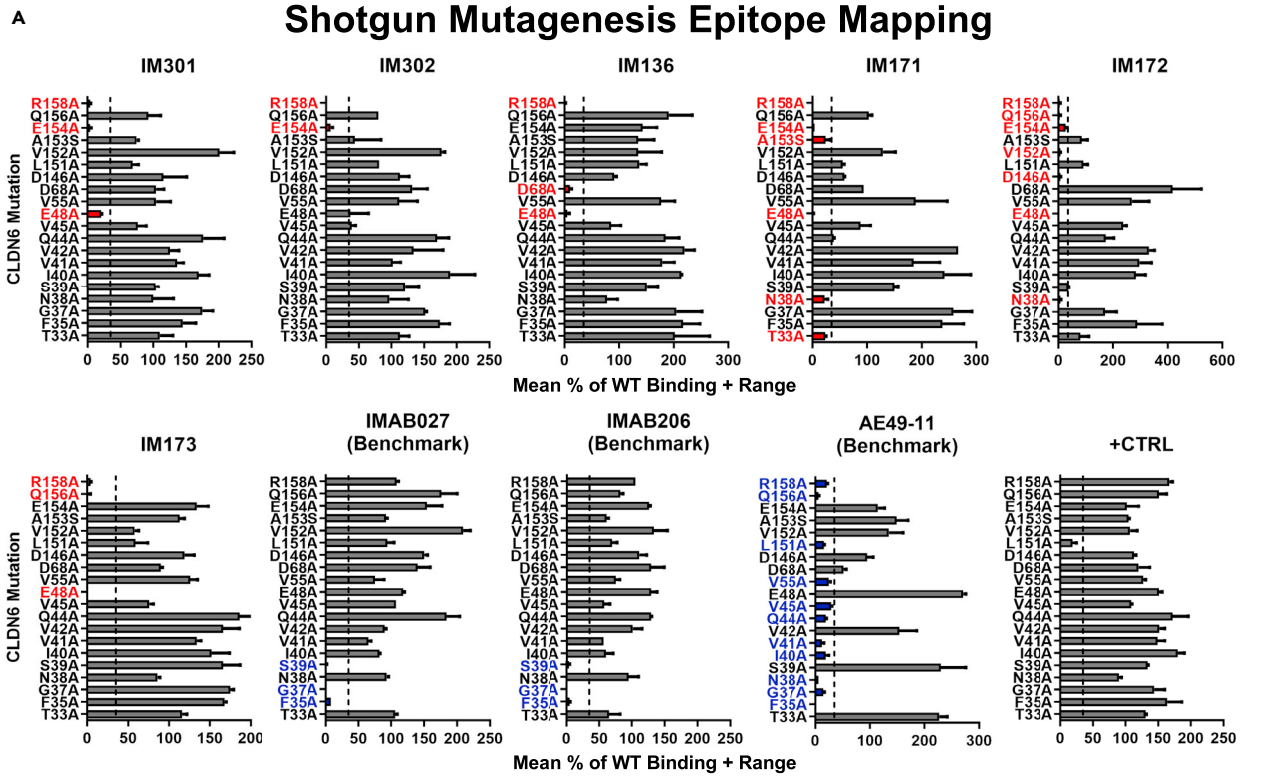
A
Shotgun Mutagenesis Epitope Mapping
IM301
IM302
IM136
IM171
IM172
IM173
IMAB027 (Benchmark)
IMAB206 (Benchmark)
AE49-11 (Benchmark)
+CTRL
CLDN6 Mutation
Mean % of WT Binding + Range

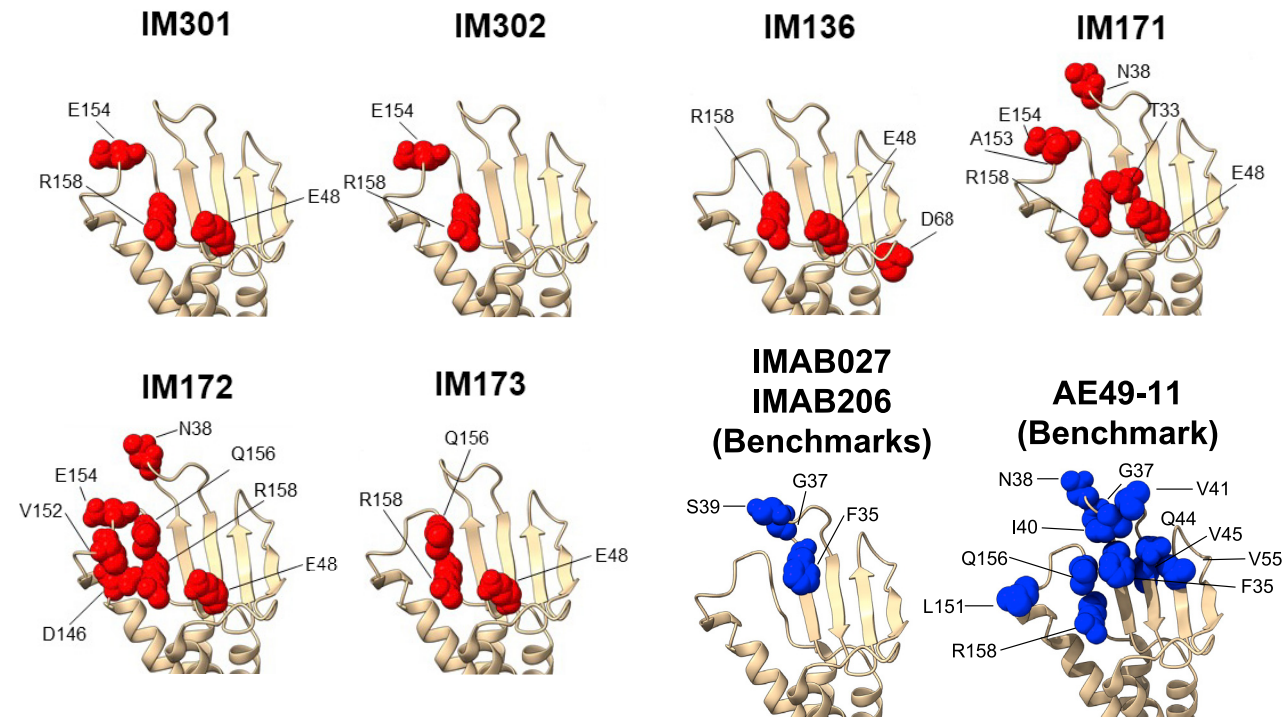
B
Critical Epitope Residues
IM301
IM302
IM136
IM171
IM172
IM173
IMAB027
IMAB206
(Benchmarks)
AE49-11
(Benchmark)

Figure 6. Epitope mapping at single amino acid resolution

(A) Critical residues for MAb binding were identified by shotgun mutagenesis alanine scanning across CLDN6. MAb binding was assessed by flow cytometry of each MAb against each of 219 individual mutations expressed in HEK-293T cells. A residue was considered critical if it resulted in <35% of binding signal relative to wild-type CLDN6, with control MAbs binding to the same mutation at wild-type levels. A commercially available MAb served as positive control (+CTRL). IMAB027, IMAb206, and AE49-11 served as benchmarks. Error bars depict half the range (highest minus lowest binding value) of at least two measurements.

(B) Epitope residues are shown on a CLDN6 model based on the CLDN9 crystal structure (PDB# 6OV2, extracellular domain shown).

the Fc should not affect CLDN6 specificity. The near identity of CLDN6 and CLDN9 means that there is a very narrow structural window for achieving specificity for any CLDN6 MAb. Nevertheless, there may be other mechanisms of specificity achieved by other CLDN6 MAbs, aside from the unique mechanism that we

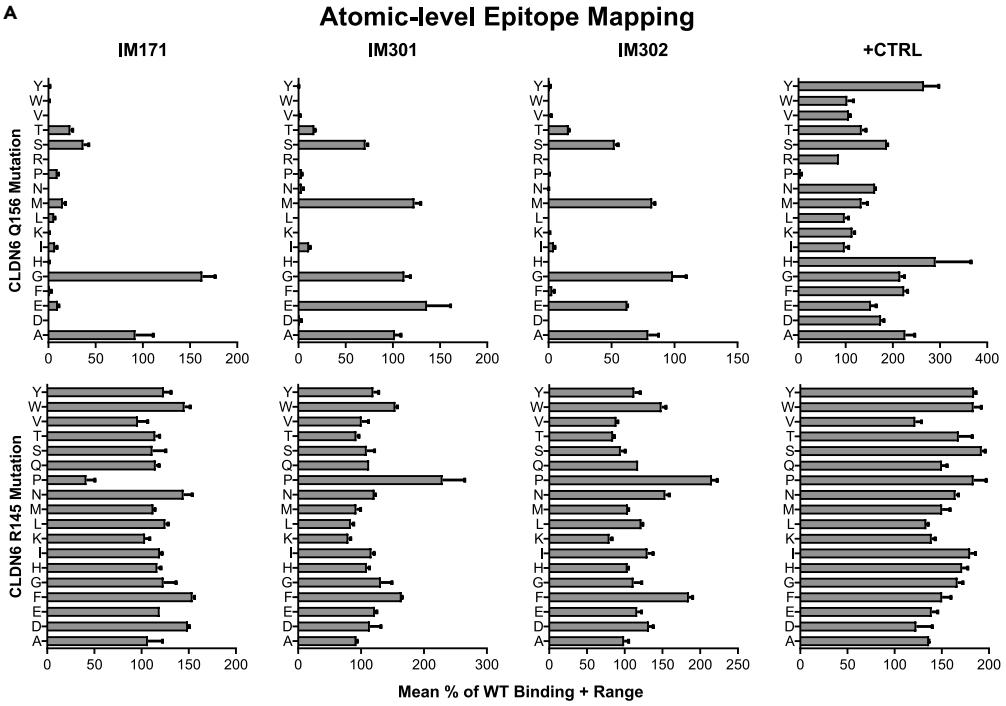

Figure 7. Atomic-level epitope mapping reveals essential role for Q156 γ carbon in determining MAb specificity for CLDN6

(A) Q156 was mutated to every other possible residue except cysteine, and tested for binding against IM171, IM301, and IM302 via flow cytometry. A commercially available MAb served as positive control (+CTRL). Error bars depict half the range (highest minus lowest binding value) of at least two measurements.

(B) Q156 occupies a central position in the CLDN6 epitope region but does not bind these MAbs directly.

(C) Shotgun mutagenesis comprehensive mutagenesis of residue Q156 reveals that binding of CLDN6-specific MAbs is inhibited by mutation to residues with branches from the β (T, V, I, P) and γ carbon (L, D, N), as well as residues with bulkier side chains (K, R, F, Y, W, H).

(D) At position 156, CLDN9 has a leucine (L), whose branching γ carbon sterically inhibits binding of CLDN6-specific MAbs.

have identified using the γ carbon of Q156. Although our CLDN6 MAbs demonstrate all critical elements necessary to become a successful therapeutic, including high specificity, high affinity, and high developability characteristics, their ability to mediate tumor killing *in vivo* remains to be published (in progress).

STAR★METHODS

Detailed methods are provided in the online version of this paper and include the following:

- KEY RESOURCES TABLE
- RESOURCE AVAILABILITY
  - Lead contact
  - Materials availability
  - Data and code availability
- EXPERIMENTAL MODEL AND SUBJECT DETAILS
  - Cell lines
- METHOD DETAILS
  - Lipoparticle generation and CLDN6 MAb isolation
  - Size exclusion chromatography
  - Differential scanning fluorimetry
  - Flow cytometry
  - Western blot
  - Immunofluorescence and confocal imaging
  - Biolayer interferometry
  - MPA Specificity Testing
  - Shotgun mutagenesis epitope mapping
- QUANTIFICATION AND STATISTICAL ANALYSIS

SUPPLEMENTAL INFORMATION

Supplemental information can be found online at https://doi.org/10.1016/j.isci.2022.105665.

ACKNOWLEDGMENTS

We thank Ginny Feltzin for writing and editorial assistance; Soma Banik, Alyssa Cunningham, Edgar Davidson, Kyle Doolan, Rachel Fong, Jennifer Houtmann, Manu Mabila, Diana Norden, Nnenna Nwogu, Duncan Paterson, Riley Payne, Meghan Pitts, Hayley Roth, Tabb Sullivan, Sharon Willis, Patrick Zeniecki, McKayla Zimmerman, and Austin Zimmet for technical assistance, scientific advice, and discussions.

AUTHOR CONTRIBUTIONS

Conceptualization, B.S, T.C., B.J.D., J.B.R., and R.C.; Investigation, B.S., L.J.S., T.B., K.S., S.G., R.W., S.A., T.P., C.A., K.S., P.M., D.B.H., and T.C.; Writing – Original Draft, B.J.D.; Writing – Review and Editing, B.J.D., J.B.R., and R.C.; Supervision, B.J.D., J.B.R., and R.C.

DECLARATION OF INTERESTS

B.J.D. and J.B.R. are shareholders of Integral Molecular. B.S., L.J.S., T.B., T.C., B.J.D., J.B.R., and R.C. have a patent related to the antibodies generated in this work, patent WO2020168059A1.

Received: April 13, 2022
Revised: September 20, 2022
Accepted: November 21, 2022
Published: December 22, 2022

REFERENCES

1. Günzel, D., and Yu, A.S.L. (2013). Claudins and the modulation of tight junction permeability. Physiol. Rev. *93*, 525–569.

2. Morin, P.J. (2005). Claudin proteins in human cancer: promising new targets for diagnosis and therapy. Cancer Res. *65*, 9603–9606.

3. Martin, T.A., and Jiang, W.G. (2001). Tight junctions and their role in cancer metastasis. Histol. Histopathol. *16*, 1183–1195.

4. Kwon, M.J. (2013). Emerging roles of claudins in human cancer. Int. J. Mol. Sci. *14*, 18148–18180.

5. Anderson, W.J., Zhou, Q., Alcalde, V., Kaneko, O.F., Blank, L.J., Sherwood, R.I., Guseh, J.S., Rajagopal, J., and Melton, D.A. (2008). Genetic

targeting of the endoderm with claudin-6CreER. Dev. Dynam. *237*, 504–512.

6. Wang, L., Xue, Y., Shen, Y., Li, W., Cheng, Y., Yan, X., Shi, W., Wang, J., Gong, Z., Yang, G., et al. (2012). Claudin 6: a novel surface marker for characterizing mouse pluripotent stem cells. Cell Res. *22*, 1082–1085.

7. Hewitt, K.J., Agarwal, R., and Morin, P.J. (2006). The claudin gene family: expression in normal and neoplastic tissues. BMC Cancer *6*, 186.

8. Sullivan, L.M., Yankovich, T., Le, P., Martinez, D., Santi, M., Biegel, J.A., Pawel, B.R., and Judkins, A.R. (2012). Claudin-6 is a nonspecific marker for malignant rhabdoid and other pediatric tumors. Am. J. Surg. Pathol. *36*, 73–80.

9. Birks, D.K., Kleinschmidt-DeMasters, B.K., Donson, A.M., Barton, V.N., McNatt, S.A., Foreman, N.K., and Handler, M.H. (2010). Claudin 6 is a positive marker for atypical teratoid/rhabdoid tumors. Brain Pathol. *20*, 140–150.

10. Rendón-Huerta, E., Teresa, F., Teresa, G.M., Xochitl, G.-S., Georgina, A.-F., Veronica, Z.-Z., and Montaño, L.F. (2010). Distribution and expression pattern of claudins 6, 7, and 9 in diffuse- and intestinal-type gastric adenocarcinomas. J. Gastrointest. Cancer *41*, 52–59.

11. Lal-Nag, M., Battis, M., Santin, A.D., and Morin, P.J. (2012). Claudin-6: a novel receptor for CPE-mediated cytotoxicity in ovarian cancer. Oncogenesis *1*, e33.

12. Yafang, L., Qiong, W., Yue, R., Xiaoming, X., Lina, Y., Mingzi, Z., Ting, Z., Yulin, L., and Chengshi, Q. (2011). Role of estrogen receptor-α in the regulation of claudin-6 expression in breast cancer cells. J. Breast Cancer *14*, 20–27.

13. Kohmoto, T., Masuda, K., Shoda, K., Takahashi, R., Ujiro, S., Tange, S., Ichikawa, D., Otsuji, E., and Imoto, I. (2020). Claudin-6 is a single prognostic marker and functions as a tumor-promoting gene in a subgroup of intestinal type gastric cancer. Gastric Cancer *23*, 403–417.

14. Micke, P., Mattsson, J.S.M., Edlund, K., Lohr, M., Jirström, K., Berglund, A., Botling, J., Rahnenfuehrer, J., Marincevic, M., Pontén, F., et al. (2014). Aberrantly activated claudin 6 and 18.2 as potential therapy targets in non-small-cell lung cancer. Int. J. Cancer *135*, 2206–2214.

15. Wang, L., Jin, X., Lin, D., Liu, Z., Zhang, X., Lu, Y., Liu, Y., Wang, M., Yang, M., Li, J., and Quan, C. (2013). Clinicopathologic significance of claudin-6, occludin, and matrix metalloproteinases −2 expression in ovarian carcinoma. Diagn. Pathol. *8*, 190.

16. Turksen, K., and Troy, T.C. (2001). Claudin-6: a novel tight junction molecule is developmentally regulated in mouse embryonic epithelium. Dev. Dynam. *222*, 292–300.

17. Tang, Z., Li, C., Kang, B., Gao, G., Li, C., and Zhang, Z. (2017). GEPIA: a web server for cancer and normal gene expression profiling and interactive analyses. Nucleic Acids Res. *45*, W98–W102.

18. Sievers, F., and Higgins, D.G. (2014). Clustal Omega, accurate alignment of very large numbers of sequences. Methods Mol. Biol. *1079*, 105–116.

19. Letunic, I., and Bork, P. (2007). Interactive Tree of Life (iTOL): an online tool for phylogenetic tree display and annotation. Bioinformatics *23*, 127–128.

20. Cancer Genome Atlas Research Network, Weinstein, J.N., Collisson, E.A., Mills, G.B., Shaw, K.R.M., Ozenberger, B.A., Ellrott, K., Shmulevich, I., Sander, C., and Stuart, J.M. (2013). The cancer genome atlas pan-cancer analysis project. Nat. Genet. *45*, 1113–1120.

21. Zavala-Zendejas, V.E., Torres-Martinez, A.C., Salas-Morales, B., Fortoul, T.I., Montaño, L.F., and Rendon-Huerta, E.P. (2011). Claudin-6, 7, or 9 overexpression in the human gastric adenocarcinoma cell line AGS increases its invasiveness, migration, and proliferation rate. Cancer Invest. *29*, 1–11.

22. Sallinen, H., Janhonen, S., Pölönen, P., Niskanen, H., Liu, O.H., Kivelä, A., Hartikainen, J.M., Anttila, M., Heinäniemi, M., Ylä-Herttuala, S., and Kaikkonen, M.U. (2019). Comparative transcriptome analysis of matched primary and distant metastatic ovarian carcinoma. BMC Cancer *19*, 1121.

23. Lal-Nag, M., and Morin, P.J. (2009). The claudins. Genome Biol. *10*, 235.

24. Colegio, O.R., Van Itallie, C.M., McCrea, H.J., Rahner, C., and Anderson, J.M. (2002). Claudins create charge-selective channels in the paracellular pathway between epithelial cells. Am. J. Physiol. Cell Physiol. *283*, C142–C147.

25. Angelow, S., Ahlstrom, R., and Yu, A.S.L. (2008). Biology of claudins. Am. J. Physiol. Ren. Physiol. *295*, F867–F876.

26. Piontek, J., Winkler, L., Wolburg, H., Müller, S.L., Zuleger, N., Piehl, C., Wiesner, B., Krause, G., and Blasig, I.E. (2008). Formation of tight junction: determinants of homophilic interaction between classic claudins. Faseb. J. *22*, 146–158.

27. Vecchio, A.J., and Stroud, R.M. (2019). Claudin-9 structures reveal mechanism for toxin-induced gut barrier breakdown. Proc. Natl. Acad. Sci. USA *116*, 17817–17824.

28. Tucker, D.F., Sullivan, J.T., Mattia, K.A., Fisher, C.R., Barnes, T., Mabila, M.N., Wilf, R., Sulli, C., Pitts, M., Payne, R.J., et al. (2018). Isolation of state-dependent monoclonal antibodies against the 12-transmembrane domain glucose transporter 4 using virus-like particles. Proc. Natl. Acad. Sci. USA *115*, E4990–E4999.

29. Balliet, J.W., and Bates, P. (1998). Efficient infection mediated by viral receptors incorporated into retroviral particles. J. Virol. *72*, 671–676.

30. Endres, M.J., Jaffer, S., Haggarty, B., Turner, J.D., Doranz, B.J., O'Brien, P.J., Kolson, D.L., and Hoxie, J.A. (1997). Targeting of HIV- and SIV-infected cells by CD4-chemokine receptor pseudotypes. Science *278*, 1462–1464.

31. Hoffman, T.L., Canziani, G., Jia, L., Rucker, J., and Doms, R.W. (2000). A biosensor assay for studying ligand-membrane receptor interactions: binding of antibodies and HIV-1 Env to chemokine receptors. Proc. Natl. Acad. Sci. USA *97*, 11215–11220.

32. Finlay, W.J.J., Bloom, L., and Cunningham, O. (2011). Optimized generation of high-affinity, high-specificity single-chain Fv antibodies from multiantigen immunized chickens. Methods Mol. Biol. *681*, 383–401.

33. Wu, L., Oficjalska, K., Lambert, M., Fennell, B.J., Darmanin-Sheehan, A., Ní Shúilleabháin, D., Autin, B., Cummins, E., Tchistiakova, L., Bloom, L., et al. (2012). Fundamental characteristics of the immunoglobulin VH repertoire of chickens in comparison with those of humans, mice, and camelids. J. Immunol. *188*, 322–333.

34. Türeci, Ö., Kreuzberg, M., Walter, K., Wöll, S., Schmitt, R., Mitnacht-Kraus, R., Nakajo, I., Yamada, T., and Sahin, U. (2018). Abstract 882: the anti-claudin 6 antibody, IMAB027, induces antibody-dependent cellular and complement-dependent cytotoxicity in claudin 6-expressing cancer cells. Cancer Res. *78*, 882.

35. Boswell, C.A., Tesar, D.B., Mukhyala, K., Theil, F.P., Fielder, P.J., and Khawli, L.A. (2010). Effects of charge on antibody tissue distribution and pharmacokinetics. Bioconjugate Chem. *21*, 2153–2163.

36. Jain, T., Sun, T., Durand, S., Hall, A., Houston, N.R., Nett, J.H., Sharkey, B., Bobrowicz, B., Caffry, I., Yu, Y., et al. (2017). Biophysical properties of the clinical-stage antibody landscape. Proc. Natl. Acad. Sci. USA *114*, 944–949.

37. Jefferis, R. (2016). Posttranslational modifications and the immunogenicity of biotherapeutics. J. Immunol. Res. *2016*, 5358272.

38. Gerhart, J., Bowers, J., Gugerty, L., Gerhart, C., Martin, M., Abdalla, F., Bravo-Nuevo, A., Sullivan, J.T., Rimkunas, R., Albertus, A., et al. (2020). Brain-specific angiogenesis inhibitor 1 is expressed in the Myo/Nog cell lineage. PLoS One *15*, e0234792.

39. Huston-Paterson, D.J., Banik, S.S., and Doranz, B.J. (2016). Screening the membrane proteome: a high-throughput platform for identifying membrane protein antibody targets. Genet. Eng. Biotechnol. News *36*, 18–19.

40. Li, W., Schäfer, A., Kulkarni, S.S., Liu, X., Martinez, D.R., Chen, C., Sun, Z., Leist, S.R., Drelich, A., Zhang, L., et al. (2020). High potency of a bivalent human V(H) domain in SARS-CoV-2 animal models. Cell *183*, 429–441.e16.

41. Radhakrishnan, S.V., Luetkens, T., Scherer, S.D., Davis, P., Vander Mause, E.R., Olson, M.L., Yousef, S., Panse, J., Abdiche, Y., Li, K.D., et al. (2020). CD229 CAR T cells

eliminate multiple myeloma and tumor propagating cells without fratricide. Nat. Commun. *11*, 798.

42. Norden, D.M., and Doranz, B.J. (2021). Testing for off-target binding. In Translational Medicine - Optimizing Preclinical Safety Evaluation of Biopharmaceuticals: Principles, Practices, and Practical Applications, J. Cavagnaro and M.E. Cosenza, eds. (CRC Press).

43. Davidson, E., and Doranz, B.J. (2014). A high-throughput shotgun mutagenesis approach to mapping B-cell antibody epitopes. Immunology *143*, 13–20.

44. Garces, F., Mohr, C., Zhang, L., Huang, C.S., Chen, Q., King, C., Xu, C., and Wang, Z. (2020). Molecular insight into recognition of the CGRPR complex by migraine prevention therapy aimovig (Erenumab). Cell Rep. *30*, 1714–1723.e6.

45. Rondeau, J.M., Ramage, P., Zurini, M., and Gram, H. (2015). The molecular mode of action and species specificity of canakinumab, a human monoclonal antibody neutralizing IL-1β. mAbs *7*, 1151–1160.

46. Soliman, C., Chua, J.X., Vankemmelbeke, M., McIntosh, R.S., Guy, A.J., Spendlove, I., Durrant, L.G., and Ramsland, P.A. (2020). The terminal sialic acid of stage-specific embryonic antigen-4 has a crucial role in binding to a cancer-targeting antibody. J. Biol. Chem. *295*, 1009–1020.

47. Fleming, J.K., Wojciak, J.M., Campbell, M.A., and Huxford, T. (2011). Biochemical and structural characterization of lysophosphatidic acid binding by a humanized monoclonal antibody. J. Mol. Biol. *408*, 462–476.

48. Stadler, C.R., Bähr-Mahmud, H., Plum, L.M., Schmoldt, K., Kölsch, A.C., Türeci, Ö., and Sahin, U. (2016). Characterization of the first-in-class T-cell-engaging bispecific single-chain antibody for targeted immunotherapy of solid tumors expressing the oncofetal protein claudin 6. OncoImmunology *5*, e1091555.

49. Stadler, C.R., Bähr-Mahmud, H., Celik, L., Hebich, B., Roth, A.S., Roth, R.P., Karikó, K., Türeci, Ö., and Sahin, U. (2017). Elimination of large tumors in mice by mRNA-encoded bispecific antibodies. Nat. Med. *23*, 815–817.

50. Hamilton, E., Fleming, G.F., Thaker, P.H., Subbiah, V., Chen, C., Fong, A., Brickman, D., and Moore, K. (2020). Abstract CT124: first-in-human study of SC-004, an antibody-drug conjugate targeting CLDN6/9, in patients with epithelial ovarian cancers. Cancer Res. *80*, CT124.

51. Reinhard, K., Rengstl, B., Oehm, P., Michel, K., Billmeier, A., Hayduk, N., Klein, O., Kuna, K., Ouchan, Y., Wöll, S., et al. (2020). An RNA vaccine drives expansion and efficacy of claudin-CAR-T cells against solid tumors. Science *367*, 446–453.

52. Drago, J.Z., Modi, S., and Chandarlapaty, S. (2021). Unlocking the potential of antibody–drug conjugates for cancer therapy. Nat. Rev. Clin. Oncol. *18*, 327–344.

53. Labrijn, A.F., Janmaat, M.L., Reichert, J.M., and Parren, P.W.H.I. (2019). Bispecific antibodies: a mechanistic review of the pipeline. Nat. Rev. Drug Discov. *18*, 585–608.

54. Suurs, F.V., Lub-de Hooge, M.N., de Vries, E.G.E., and de Groot, D.J.A. (2019). A review of bispecific antibodies and antibody constructs in oncology and clinical challenges. Pharmacol. Ther. *201*, 103–119.

55. Morgan, R.A., Yang, J.C., Kitano, M., Dudley, M.E., Laurencot, C.M., and Rosenberg, S.A. (2010). Case report of a serious adverse event following the administration of T cells transduced with a chimeric antigen receptor recognizing ERBB2. Mol. Ther. *18*, 843–851.

56. Willis, S., Davidoff, C., Schilling, J., Wanless, A., Doranz, B.J., and Rucker, J. (2008). Virus-like particles as quantitative probes of membrane protein interactions. Biochemistry *47*, 6988–6990.

57. Paes, C., Ingalls, J., Kampani, K., Sulli, C., Kakkar, E., Murray, M., Kotelnikov, V., Greene, T.A., Rucker, J.B., and Doranz, B.J. (2009). Atomic-level mapping of antibody epitopes on a GPCR. J. Am. Chem. Soc. *131*, 6952–6954.

58. Pettersen, E.F., Goddard, T.D., Huang, C.C., Couch, G.S., Greenblatt, D.M., Meng, E.C., and Ferrin, T.E. (2004). UCSF Chimera–a visualization system for exploratory research and analysis. J. Comput. Chem. *25*, 1605–1612.

STAR★METHODS

KEY RESOURCES TABLE

REAGENT or RESOURCE	SOURCE	IDENTIFIER
Antibodies		
IMAB027	this manuscript	Patent US932842
IMAB206	this manuscript	Patent WO 2018/054,484 A1
AE49011	this manuscript	Patent EP3064512A2
IM301	this manuscript	N/A
IM302	this manuscript	N/A
IM171	this manuscript	N/A
IM172	this manuscript	N/A
IM173	this manuscript	N/A
IM136	this manuscript	N/A
Anti-Claudin6	Abcam	Cat# Ab99226; RRID: AB_10861897
Anti-Claudin6	R&D Systems	Cat# MAB3656; RRID: AB_2292076
Anti-P2X3	this manuscript	N/A
APC AffiniPure goat anti-human IgG	Jackson ImmunoResearch	Cat# 109-135-098; RRID: AB_2337690
Alexa Fluor 647 AffiniPure goat anti-human IgG	Jackson ImmunoResearch	Cat# 109-605-003; RRID: AB_2337880
Alexa Fluor 488 goat anti-human IgG	Jackson ImmunoResearch	Cat# 109-545-003; RRID: AB_2337831
PerCP Streptavidin	Biolegend	Cat# 405213
HRP conjugated anti-rabbit IgG	Southern Biotech	Cat# 4050-05; RRID: AB_2795955
HRP conjugated anti-human IgG	Southern Biotech	Cat# 6140-05; RRID: AB_2796197
Bacterial and virus strains		
E.coli NEB 5-alpha	New England Biolabs	Cat# C29871
Chemicals, peptides, and recombinant proteins		
Lipoparticles	This manuscript	N/A
Trypsin	Corning	Cat# 25-052-CV
Lipofectamine 2000	Thermo Fisher	Cat# 11668500
ExpiFectamine	Gibco	Cat# A14524
SEC protein standard mix	Sigma	Cat# 69385
BCA Protein Assay kit	Thermo Fisher Scientific	Cat# P123223, P123224, 23,209
Critical commercial assays		
Intellicyt high throughput flow cytometer	Sartorius	iQue3
SuperSignal™ West Pico PLUS Chemiluminescent Substrate	ThermoFisher Scientific	Cat# 34580
MabSelect SuRe	Cytiva	Cat# 1754803
Superdex 200 Increase 3.$^{2}/_{3}$00 column	GE	Cat# 29-0272-72
AKTA Pure fast protein liquid chromatography system	Cytiva	N/A
CellInsight CX7 High-Content Screening Plat-form	Thermo Scientific	Cat# HCSDCX7LEDPRO
ForteBio Octet Red biosensor system	Pall-ForteBio, Inc	N/A
Membrane Proteome Array	Integral Molecular	N/A
Pierce Femto kit	Pierce	Cat# 34095
iQ5 Thermocycler	BioRad	N/A
Imaging System	Bio-Rad	ChemiDoc

(*Continued on next page*)

Continued

REAGENT or RESOURCE	SOURCE	IDENTIFIER
Experimental models: Cell lines		
HEK-293T	ATCC	Cat# CRL-3216
HEK-293F	Gibco	Cat# R79007
A549	ATCC	Cat# CCL-185
ExpiCHO-S	Gibco	Cat# A29127
OVCAR3	ATCC	Cat# HTB-161
OV90	ATCC	Cat# CRL-11732
PA-1	ATCC	Cat# CRL-1572
Recombinant DNA		
Claudin 6 mutant library	This manuscript	N/A
Claudin 3, 4, 6, 9 expression constructs	This manuscript	N/A
Software and algorithms		
GraphPad Prism Graphing software	GraphPad	v 9.0.0
PDB	rcsb.org	6OV2
Structure Visualization Software	https://www.cgl.ucsf.edu/chimera	UCSF Chimera
Octet data analysis	ForteBio	V8.1
Other		
Saponin	VWR	Cat# TCS0019-025G
DMEM	Fisher Scientific	Cat# MT10017CM
Sodium pyruvate	VWR	Cat# 45000-710
L-Alanyl-L-Glutamine	VWR	Cat# 45001-086
HEPES	VWR	Cat# 45000-690
Penicillin-Streptomycin	Fisher Scientific	Cat# 15-140-163
Paraformaldehyde	VWR	Cat# 100496-496
Donor Goat Serum	Atlanta Biologicals	Cat# S13150
Pluronic	Fisher Scientific	Cat# 24-040-032
DPBS(++)	Cytiva	Cat# SH30264.02
PBS	ThermoFisher	Cat# SH30256.01
DAPI	ThermoFisher	Cat# D12490
SYPRO Orange dye	Sigma-Aldrich	Cat# S5692
Laemmli	Bio-Rad	Cat# 1610737EDU
Cellstripper	Corning	Cat# 25-056-CI
Goat Serum	R&D Systems	Cat# S13150
Acrylamide gradient gel	Nusep	Cat# NN12-420
PVDF membrane	VWR	Cat# 28165-512
Precision plus Protein Dual Color Standards	BioRad	Cat# 61-0374

RESOURCE AVAILABILITY

Lead contact

Further information and requests for resources and reagents should be directed to and will be fulfilled by the lead contact, Ross Chambers (rchambers@integralmolecular.com).

Materials availability

Lipoparticles and Shotgun Mutagenesis mutation libraries generated in this study are available on a commercial basis from Integral Molecular. The antibodies described in this manuscript are patented and subject to restrictions due to active licensing agreements.

Data and code availability

All data reported in this paper will be shared by the lead contact upon reasonable request. Original code is not reported in the paper. Any additional information required to reanalyze the data reported in this paper is available from the lead contact upon request.

EXPERIMENTAL MODEL AND SUBJECT DETAILS

Cell lines

HEK-293T, A549, OVCAR3, OV90, and PA-1 cells were originally obtained from AmericanType Culture Collection (ATCC). HEK-293F and ExpiCHO-S cells were obtained from Gibco. All cells were cultured in the recommended medium supplemented with 10% fetal bovine serum (FBS) and penicillin-streptomycin (100 U/mL) at 37°C in 5% CO2. All cell lines tested negative for mycoplasma contamination before use.

METHOD DETAILS

Lipoparticle generation and CLDN6 MAb isolation

Lipoparticles (virus-like particles) incorporating structurally intact CLDN6 were prepared as previously described by transfecting HEK-293T cells with a plasmid encoding CLDN6, other CLDNs, or no target (for null Lipoparticle control), and a plasmid encoding retroviral (MLV) Gag protein.[31,56] Chicken hosts were immunized with CLDN6 DNA (4 injections of 300μg) followed by CLDN6 Lipoparticles (150μg followed by 300μg). Successful immunization was confirmed with flow cytometry, and B cells from immunized chickens were used to generate an scFv phage display library as previously described.[32] Phage panning was carried out by allowing the phage library to bind to wells coated with CLDN6 or CLDN9, for positive selection or deselection, respectively. Bound phage were trypsin eluted and amplified for a total of 3 rounds of panning. For screening, individual phage colonies were induced by incubation in glucose-free medium at 30°C overnight, and the periplasmic fraction was extracted by freeze–thaw, then tested for CLDN6 binding by flow cytometry. For IgG MAb production, ExpiCHO cells were transfected with MAb DNA using ExpiFectamine (Gibco A14524) and incubated 7 days at 37°C. Cell supernatant was harvested and MAbs were purified using MabSelect SuRe antibody purification resin (Cytiva, 17,543,803).

Size exclusion chromatography

Samples were run on an Superdex 200 Increase 3.$^{2}/_{3}$00 column (GE 29-0272-72), using an AKTA Pure fast protein liquid chromatography system (Cytvia) at a flow rate of 0.068 mL/min and mobile phase containing 200 mM sodium phosphate and 250 mM sodium chloride at pH 7. For each antibody, 30 μL of a 0.5 mg/mL solution were injected, and the 280 nm absorbance of eluting fractions was validated against a 15–600 kDA SEC protein standard mix (Sigma 69,385).

Differential scanning fluorimetry

Samples were prepared by mixing 20 μL of 0.1 mg/mL antibody solution in PBS (−) (ThermoFisher SH30256.01) with 10 μL of 20X SYPRO Orange dye (Sigma-Aldrich, S5692) in PBS (−). Protein denaturation was performed using an iQ5 Thermocycler (BioRad) by increasing well temperature from 45°C to 95°C in increments of 0.1°C, holding at each increment for 10 s. The measurement was performed in triplicate for each antibody and melting temperature was calculated as the mean ± SD of a Gaussian fit of the first derivative of the fluorescence (470 nm excitation, 570 nm emission) vs temperature curve.

Flow cytometry

HEK-293F cells were plated at 750,000 cells per well in six-well tissue culture plates (Falcon) and transfected with CLDN6, CLDN9, CLDN3, or CLDN4 constructs and co-transfected with GFP by calcium phosphate precipitations. At 48h post transfection, successful transfection was confirmed by observing GFP fluorescence, and cells were stained with the candidate MAbs followed by biotinylated goat anti-human IgG (1:500) and streptavidin PerCP (Biolegend, 1:500) or candidate MAbs followed by APC goat anti-human IgG (1:500). Fluorescence was measured using an Intellicyt high-throughput flow cytometer (HTFC).

Western blot

Western blotting was performed using CLDN6 Lipoparticles. Total protein concentrations were calculated using a BCA Protein Assay kit (Thermo Fisher Scientific), and samples for SDS-PAGE were prepared in 2X Laemmli sample buffer (Bio-Rad) with 50 mM dithiothreitol (DTT). SDS-PAGE was performed for 2 h at 80 V

using 4-20% acrylamide gradient gels (Nusep). Proteins were transferred to PVDF membranes at room temperature (RT) for 1 h at 100 V and probed with antibodies of interest. The anti-CLDN6 linear epitope control antibody was purchased from Abcam (ab99226). Membranes were blocked in 5% fat-free milk overnight at 4°C, incubated with primary antibody (1 μg/mL) for 1 h at RT, and then for 30minat RT with a 1:5000 dilution of anti-rabbit IgG or anti-human IgG (Southern Biotech) secondary antibodies conjugated to HRP. Chemiluminescence detection was carried out using Super-Signal West Chemiluminescent Substrate (Thermo Fisher Scientific). Chemiluminescence images were collected using a 1 s exposure and processed for contrast only using ImageJ (NIH).

Immunofluorescence and confocal imaging

HEK-293F cells were transfected with CLDN6 using Lipofectamine 2000, then seeded at a density of 10,500 cells/well in a 384-well plate and incubated for 24h. Each well was washed 2X with PBS (+), fixed with 4% PFA for 10 min, and rinsed 3X with PBS (+). Each MAb was diluted to 1 μg/mL in blocking buffer containing 10% NGS in PBS (–), and cells were stained for 1 h, then washed 2X in PBS (+). Cells were stained for 30 min with Alexa Fluor 647 goat anti-human antibody diluted 1:400 in blocking buffer, washed 3X in PBS (+), fixed with 4% PFA for 10 min, and rinsed 3X with PBS (+). Cells were then stained with 0.5 μg/mL DAPI for 5 min, followed by 3 washes with PBS (+). Confocal imaging was performed using a CellInsight CX7 High-Content Screening Plat-form at 40X magnification with a pinhole size of 70 nm. Untransfected HEK-293F cells lacking endogenous CLDN6 served as a negative control.

Biolayer interferometry

Biosensor measurements were performed in PBS supplemented with 1 mg/mL BSA (PBS-B) at 25°C using a ForteBio Octet Red biosensor system (Pall-ForteBio, Inc.). Biotinylated CLDN6, CLDN9, or null Lipoparticles diluted to 20 μg/mL in PBS-B were loaded on the biosensor tip for 45 min and allowed to stabilize for 10 min. The antibody to be tested was added at varying concentrations in PBS-B, and association was measured for 5 min followed by dissociation for up to 45 min in buffer. The results were analyzed with the Octet data analysis program (v8.1; ForteBio) using a 1:2 binding model.

MPA Specificity Testing

MPA is Integral Molecular's cell-based array of ~6,000 human membrane proteins, each expressed in live unfixed cells in separate wells of a 384-well plate.[28,39] In this study, the MPA was expressed in HEK-293T cells 36h prior to testing. Each MAb was added to the MPA at a concentration of 5 μg/mL, optimized for the best signal-to-background ratio for target detection using an independent immunofluorescence titration curve against wild-type CLDN6. Binding was measured by Intellicyt iQue using a fluorescent secondary antibody. Each 384-well plate contained positive (Fc-binding) and negative (empty vector) controls to ensure plate-by-plate data validity. Hits were validated by flow cytometry with serial dilutions of antibody, and the target identity was confirmed by sequencing.

Shotgun mutagenesis epitope mapping

A comprehensive library of CLDN6 mutants was generated by performing an alanine scan along the entire length of wild-type CLDN6. Primers were designed to mutate each residue to alanine, or serine for wild-type alanine codons, resulting in 219 total mutations across the entire CLDN6 sequence (residues 2–220). All mutants were sequence confirmed, arrayed into individual wells of a 384-well plate, transfected into HEK-293T cells, and allowed to express for 22 h. Primary MAb concentrations were confirmed to be within the linear range for detection of binding using an independent immunofluorescence titration curve against wild-type CLDN6. Transfected cells were stained with IM136 at 0.5 μg/mL; IM171, IM172, and IM173 at 1.0 μg/mL; IM301 and IM302 at 0.25 μg/mL, and the IMAB027 benchmark antibody at 0.125 μg/mL. All MAb dilutions were in 10% NGS (Atlanta biologicals). Cells were then washed 2X in PBS (–), and bound MAbs were stained with an Alexa Fluor 488-conjugated secondary antibody (Jackson ImmunoResearch Laboratories) at 3.75 μg/mL in 10% NGS. Cells were washed 2X in PBS (–), monodispersed in Cellstripper solution (Corning) and then fixed with 4% paraformaldehyde (PFA; Electron Microscopy Sciences). The cells were washed 2X in PBS (–) and resuspended in Cellstripper solution with 0.2% BSA (Sigma-Aldrich) and 0.2% pluronic (Gibco), and measured for fluorescence using an Intellicyt HTFC. MAb binding signal to mutant CLDN6 was calculated by subtracting the binding signal to mock-transfected cells, normalizing to wild-type CLDN6 binding, and converting to a percentage. Residues were defined as critical if their mutation resulted in <35% binding relative to wild-type CLDN6 but did not affect the reactivity of an

expression control MAb (R&D Systems MAB3656), thus excluding mutations that cause local misfolding or expression defects.[43,57] Critical epitope residues were visualized on a CLDN6 model based on the CLDN9 crystal structure (PDB# 6OV2) using UCSF Chimera.[58]

QUANTIFICATION AND STATISTICAL ANALYSIS

Statistical details of experiments can be found in the appropriate figure legends. MAb reactivities for each alanine scan mutant are expressed as a percentage of wild-type reactivity, represent the average of at least two replicate values for each measurement, and are given and shown (Figure 6). The binding values with specific mutations are also shown (Figure 7) and are plotted with error bars depicting half the range (highest minus lowest binding value) of at least two measurements. The membrane proteome array in Figure 5 was performed with two replicates and follow-up titration curves were performed in quadruplicate at each concentration. All flow cytometry and biosensor binding kinetics experiments are performed with four replicates and values shown represent the average.